Photocatalytic Aqueous CO_2 Reduction to CO and CH_4 Sensitized by Ullazine Supramolecular Polymers

Oliver Dumele,[1,†] Luka Đorđević,[1,2,3,†] Hiroaki Sai,[2,4] Thomas J. Cotey,[4] M. Hussain Sangji,[2,5] Kohei Sato,[3] Adam J. Dannenhoffer,[4] and Samuel I. Stupp[1,2,3,4,5,6*]

[1]Department of Chemistry, Northwestern University, Evanston, IL 60208, USA

[2]Center for Bio-inspired Energy Science, Northwestern University, 2145 Sheridan Road, Evanston, IL 60208, USA

[3]Simpson Querrey Institute for BioNanotechnology, Northwestern University, Chicago, Illinois 60611, USA

[4]Department of Materials Science and Engineering, Northwestern University, Evanston, IL 60208, USA.

[5]Department of Biomedical Engineering, Northwestern University, Evanston, Illinois 60208, USA

[6]Department of Medicine, Northwestern University, Chicago, Illinois 60611, USA

[†]O.D. and L.Đ. contributed equally.

*To whom correspondence should be addressed. E-mail: s-stupp@northwestern.edu

Keywords: Ullazine, Self-Assembly, Chromophore Amphiphiles, Photocatalysis, CO_2 Reduction, Supramolecular Polymers

ABSTRACT: There has been rapid progress on the chemistry of supramolecular scaffolds that harness sunlight for aqueous photocatalytic production of hydrogen. However, great efforts are still needed to develop similar photosynthetic systems for the great challenge of CO_2 reduction especially if they avoid the use of non-abundant metals. This work investigates the synthesis of supramolecular polymers capable of sensitizing catalysts that require more negative potentials than proton reduction. The monomers are chromophore amphiphiles based on a diareno-fused ullazine core that undergo supramolecular polymerization in water to create entangled nanoscale fibers. Under 450 nm visible light these fibers sensitize a dinuclear cobalt catalyst for CO_2 photoreduction to generate carbon monoxide and methane using a sacrificial electron donor. The supramolecular photocatalytic system can generate amounts of CH_4 comparable to those obtained with a precious metal-based $[Ru(phen)_3](PF_6)_2$ sensitizer and, in contrast to Ru-based catalysts, retains photocatalytic activity in all aqueous media over 6 days. The present study demonstrates the potential of tailored supramolecular polymers as renewable energy and sustainability materials.

Introduction

Self-assembly of molecules into supramolecular materials in aqueous environments is an attractive strategy to prepare artificial photosynthetic systems.[1–7] The possibility of forming soft materials integrating all the functional elements in the form of hydrogels that mimic the environment in which natural photosynthesis occurs is an inspiring challenge for designing solar energy materials.[8–13] Such platforms generate opportunities to coat substrates with materials and perform photocatalysis in customizable solid forms as an alternative approach to traditional solution-phase systems. Also using π–π stacked supramolecular polymer scaffolds can be advantageous to help with the formation of efficient charge-separated states with long exciton lifetimes.[14] Our laboratory has reported on perylene monoimide chromophore amphiphiles that form hydrogels based on nanoscale ribbons in the presence of electrolytes that photosensitize a molecular catalyst for reduction of protons into H_2.[1,15–17] There have been other efforts in the preparation of photocatalytic systems where self-assembled organic dyes, such as perylene diimides and porphyrins, act as photosensitizers to platinum-based catalysts.[18–24] However, novel self-assembled photosensitizers are needed for powering molecular catalysts for carbon dioxide (CO_2) reduction. The photocatalytic conversion of CO_2 into chemical feedstock is attracting considerable attention as a way to address the urgent problems causing global warming and a shortage of fossil fuels.[25–29] Thus, catalytic strategies are necessary to reduce CO_2 given its inertness and the need to develop efficient and stable systems.[30–39] Reasonably high performance can be achieved in non-aqueous solvents[40–43] or water-organic solvent mixtures,[44,45] with only a few systems showing high CO_2-reducing activity in pure water.[46–48] To add one more hurdle, the ones that operate in fully aqueous media require photosensitizers containing non-abundant elements such as cadmium or ruthenium.[49,50]

We report here on a strategy to create supramolecular polymer scaffolds that integrate both light-absorbing chromophores and catalysts into materials for light-driven CO_2 reduction. Among the many polycyclic aromatic hydrocarbons reported in the literature,[51] the ullazine core (indolizino[6,5,4,3-*ija*]quinoline) was first reported in 1983 and described as a "π-excess heteroarene" due to its potential donating strength as well as electron stabilizing properties of this nitrogen-containing heterocycle.[52] Since then, ullazine derivatives have been successfully investigated as photosensitizers in dye-sensitized solar cells,[53,54] especially because of their electron-donor properties.[55] Furthermore, the synthetic approaches towards the

dibenzo[*d*,*k*]ullazine and its incorporation in larger π-conjugated systems have been recently expanded.[54,56–61] Nonetheless, the self-assembly of ullazine derivatives into supramolecular structures has been rarely studied[62] and their photoredox chemistry has yet to be explored.

Results and Discussion

Molecular Design and Synthesis. Our work aims at the design of charged amphiphiles as monomers with an excited state reduction potential high enough to sensitize molecular catalysts that require more negative potentials than the H_2 evolution reaction (Figure 1). Starting from the ullazine core, we introduced the following modifications: (*i*) formation of a chromophore amphiphile by introducing a monoimide group bearing a carboxylic acid through a five-carbon linker. While the imide group introduces a dipole moment to the π-extended core, the carboxylate is necessary as an ionizable hydrophilic head group in water; (*ii*) lateral π-extension of the ullazine core to enhance the chromophore absorption of visible light;[54] (*iii*) an *n*-pentyl tail opposite the hydrophilic vector to increase the solubility of the molecule during the synthesis and facilitate additional hydrophobic self-assembly.

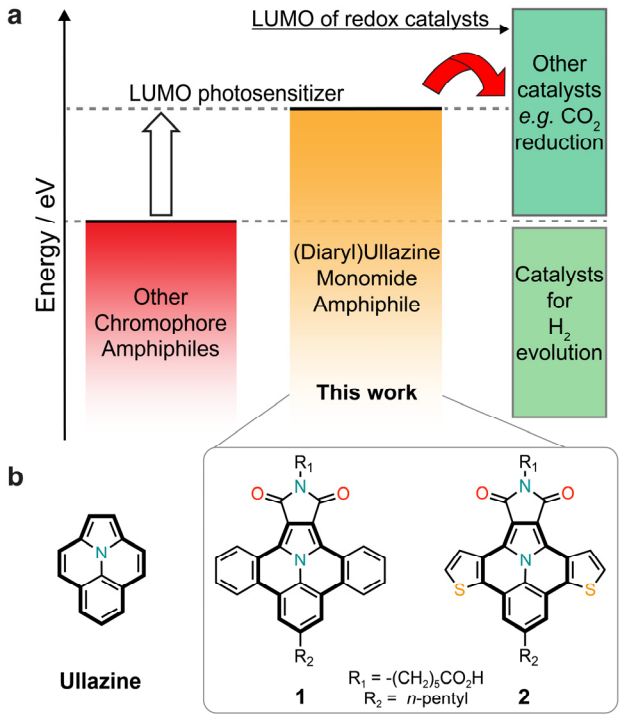

Figure 1. Schematic representation of the artificial photocatalytic systems presented in this work. **a**) Energy levels representation for the preparation of self-assembled chromophores capable of producing solar fuels beyond H_2, such as photosensitization of molecular catalysts for CO_2 reduction; **b**) chemical structures of the ullazine molecule and the two diareno-fused ullazines synthesized in this work.

For the synthesis of compounds **1** and **2** (Scheme 1), we adapted the selective 1,3-dipolar cycloaddition reaction between azomethine ylides **5** or **9** and dipolarophile *tert*-butyl 6-maleimidohexanoate.[56,63] In brief, Suzuki cross-coupling between 2,6-dibromo-4-(*n*-pentyl)aniline (**3**) and 1-hydroxy-3*H*-2,1-benzoxaborole to afford diol **4**, followed by HCl-induced microwave-assisted cyclization and oxidation by trityl tetrafluoroborate. In the case of dithieno-azomethine ylide **10**, the preparation of the diol **9** had to account for the inherent instability of 2-thienylboronic acid by exploiting its *in situ* slow-release cross-coupling from the corresponding MIDA boronate (**8**) developed by Burke and co-workers.[64] With the two azomethine ylide precursors (**5** and **10**) in hand, we performed a one-pot 1,3-dipolar cycloaddition reactions with *tert*-butyl 6-maleimidohexanoate, followed by oxidation/rearomatization of the cycloaddition intermediates with 2,3-dichloro-5,6-dicyano-1,4-benzoquinone (DDQ). Following chromatographic purifications, the *tert*-butyl esters $\mathbf{1}^{t\mathbf{Bu}}$ and $\mathbf{2}^{t\mathbf{Bu}}$ were obtained and could be quantitatively deprotected by using trifluoroacetic acid. The compounds **1** and **2** were unambiguously characterized by NMR spectroscopy, high-resolution mass spectrometry, and single-crystal X-ray crystallography (*vide infra*).

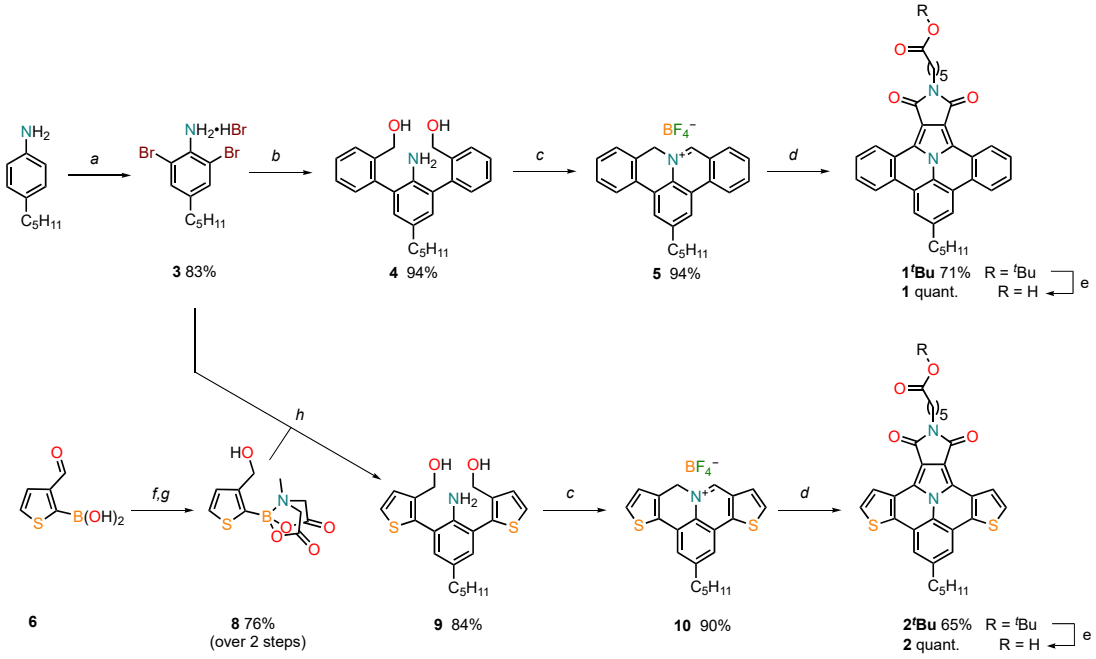

Scheme 1. Synthetic approach for the preparation of ullazine monoimide amphiphiles **1** and **2**. Reagents and conditions: **a**) Br_2, CH_3CO_2H, CH_2Cl_2, 4→25 °C; **b**) 1-hydroxy-3*H*-2,1-benzoxaborole, $[Pd(PPh_3)_4]$, K_2CO_3, H_2O/EtOH/toluene, 110 °C, N_2; **c**) step (*i*) HCl (4 M in 1,4-dioxane), μ-wave heating, 130 °C, N_2; step (*ii*) CPh_3BF_4, CH_3CN/toluene, 90 °C, N_2; **d**) step (*i*) *tert*-butyl 6-maleimidohexanoate, Et_3N, CH_2Cl_2, 25 °C, N_2; step (*ii*) DDQ, CH_2Cl_2/toluene, 25 °C, N_2; **e**) CF_3CO_2H, CH_2Cl_2, 25 °C; **f**) methyliminodiacetic acid, benzene/DMSO, 105 °C; **g**) $NaBH_4$, CH_3OH/THF, 0→4 °C; **h**) $Pd(OAc)_2$, SPhos, aq. K_3PO_4, 1,4-dioxane, 57 °C.

Photophysical and electrochemical properties of monomers. In order to determine the photophysical properties and the energy levels of ullazine derivatives **1** and **2**, we performed UV-Vis absorption and fluorescence spectroscopy, cyclic voltammetry (CV), differential pulse voltammetry (DPV), and also time-dependent density functional theory (TD-DFT) calculations. The difference between the two compounds in their monomeric form is revealed by their specific color in DMSO solutions. Compound **1** is almost colorless, while compound **2** is bright yellow (Figure 2a, inset), thus confirming that the replacement of the two annulated benzo rings with two thieno rings resulted in a red-shifted absorbance band suitable for visible-light photocatalysis. The UV-Vis absorption spectra (20 μM in DMSO, 298 K) reveal the lowest electronic transitions at 410 and 431 nm for **1** and **2**, respectively (Figure 2a). According to TD-DFT calculations, these bands are attributed to π−π* transitions (Tables S4–S5, Figures S20–S21). Emission profiles for **1** and **2** displayed mirroring luminescence profiles with narrow Stokes shifts (22 and 17 nm, respectively), and good fluorescence quantum yields (φ_{fl} = 59% and 58%, respectively).

We also investigated the aromaticity of compounds **1** and **2** computationally by nucleus-independent chemical shift (NICS)[65] and anisotropy of the induced current density (AICD)[66] analyses (Figures S22–S25). $NICS_{\pi zz}$-*X* scan and $NICS_{\pi zz}$-*XY* heat maps for compound **1** show significant local diatropic currents for the three outer benzenoid rings and the pyrrole unit, while the central 6-membered rings exhibit a non-aromatic character. In contrast, replacement of the annulated benzene rings with two thieno rings in **2** yields a globally diatropic ring current in the dithienoullazine core. These findings were further corroborated by $NICS_{\pi zz}$-*Z* scans and AICD plots (Supporting Information, Figures S23–S25).

Cyclic and differential CV and DPV were used to assess the redox properties of the ^{t}Bu-protected compounds (**1**$^{t\mathbf{Bu}}$ and **2**$^{t\mathbf{Bu}}$**)** in order to achieve the necessary solubility in organic solvents (CH_2Cl_2). The CV profiles of these compounds shown in Figure 2b reveal one reversible oxidation wave (+0.85 V for **1**$^{t\mathbf{Bu}}$ and +0.69 V for **2**$^{t\mathbf{Bu}}$ using ferrocene as internal standard), whereas only irreversible reduction waves were observed in our experimental setup (onset at −2.11 V for **1**$^{t\mathbf{Bu}}$ and −2.10 V for **2**$^{t\mathbf{Bu}}$). DPV scans allowed us to reveal these reduction potentials of −2.23 for **1**$^{t\mathbf{Bu}}$ and −2.19 V for **2**$^{t\mathbf{Bu}}$ (Supporting Information, Figure S14). Compared to the perylene monoimide chromophore amphiphile previously reported to photosensitize proton reduction catalysts

(Supporting Information, Figure S15),[1,15] the reduction potential is more negative by 0.70 V, which could be useful to sensitize catalysts that require more negative potentials than the H_2 evolution reaction (*vide infra*).

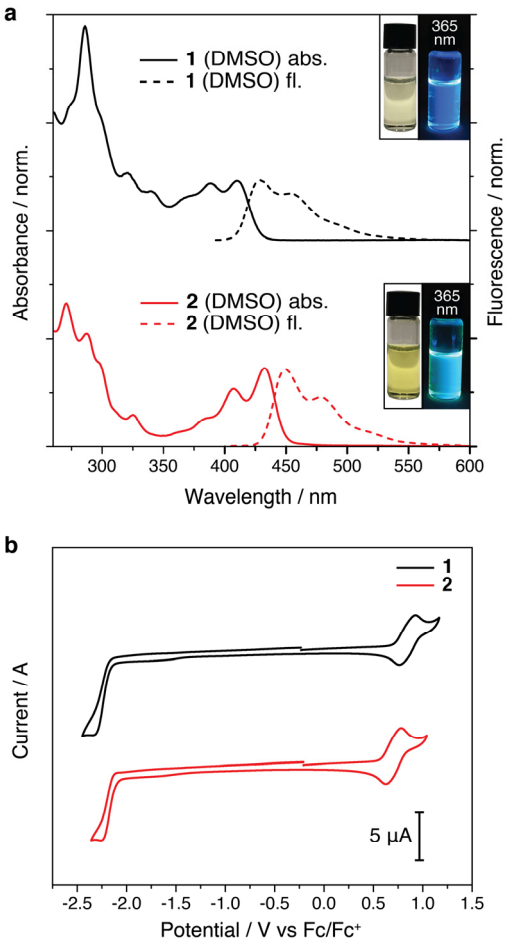

Figure 2. Photophysical and electrochemical properties of the two diareno-fused ullazine amphiphiles **1** and **2** in organic solutions. **a**) Absorption (full lines) and emission properties (dashed lines) of molecules **1** (black trace) and **2** (red trace) as DMSO solutions (20 µM) (the insets show photographs of the diarenoullazines **1** and **2** solutions under ambient light (left) and under 365 nm handheld lamp (right)); **b**) cyclic voltammograms of ^{t}Bu protected $\mathbf{1}^{t\mathbf{Bu}}$ and $\mathbf{2}^{t\mathbf{B}}$ (1 mM in CH_2Cl_2, 100 mM $TBAPF_6$, 100 mV s^{-1}, Fc/Fc^+ internal standard).

The structures of chromophores **1** and **2** were unambiguously proved by single X-ray diffraction (Figure 3). Although the crystals were grown from organic solvents, the packing between the π-extended cores gives us insights into how these molecules might assemble in aqueous solutions. Among various packing motifs (as detailed in the Supporting Information, X-ray Analysis Section S3), molecules in the crystal of **1** tend to pack in an antiparallel manner (around 3.34 Å distance

between the molecular planes), while **2** tends to adopt a 45° twist (3.39 Å distance between the molecular planes). The difference in packing modes is possibly due to the greater molecular dipole moment calculated for **1** (μ = 5.0 D) compared to that in molecule **2** (μ = 4.0 D) due to the sulfur atoms (Figure S17).

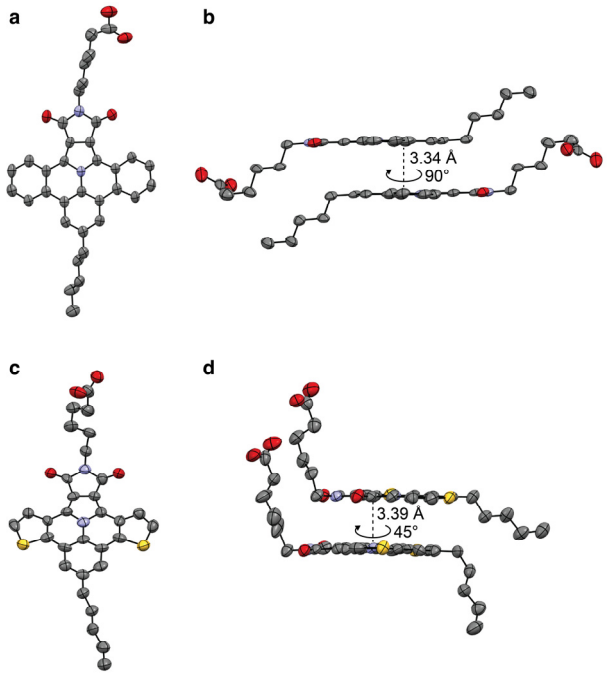

Figure 3. Single X-ray diffraction of the two diareno-fused ullazine amphiphiles **1** and **2.** Ellipsoid representation of X-ray structures of **1** (a) and **2** (c) at 100 K, 50% probability; molecular packing of selected dimers in the X-ray crystal structure of **1** (b) and **2** (d) with their stacking distance and torsional stacking angle of the chromophore cores.

Aqueous Self-Assembly. The free acids of **1** and **2** were dissolved using an equimolar amount of NaOH, followed by the addition of 300 mM NaCl (50 mM final salt concentration, 15 mM final concentration of the chromophore amphiphile). Two gels were obtained after annealing at 95 °C for 30 min, followed by slow cooling to room temperature. Besides the vial inversion test, the formation of the rather weak hydrogels was confirmed by rheological measurements (Supporting Information, Figure S33). The UV-Vis absorption and fluorescence spectra of the non-assembled monomers **1** and **2** as dilute solutions in DMSO exhibit significant vibronic bands with small Stokes shifts (Figure 2a). In contrast, the gels formed by self-assembled chromophore amphiphiles **1** and **2** show broad absorption and emission profiles (Figure 4). Additionally, compared to the monomeric species in DMSO, the absorption and emission profiles are red-shifted with λ_{max} = 428

nm (onset estimated at 465 nm) for self-assembled versus 410 nm for monomeric **1**. Similarly, dithienoullazine **2** showed a red-shift from λ_{max} = 431 nm for its monomeric state to λ_{max} = 449 nm for its gelled state (with an onset at 502 nm). We found the fluorescence emission follows a similar trend with λ_{em} = 516 nm and λ_{em} = 542 nm for self-assembled compounds **1** and **2**, respectively, indicating the stacking of ullazine amphiphiles in water through self-assembly affords the capture of a wider energy range of visible light photons through red-shifting and spectral broadening.

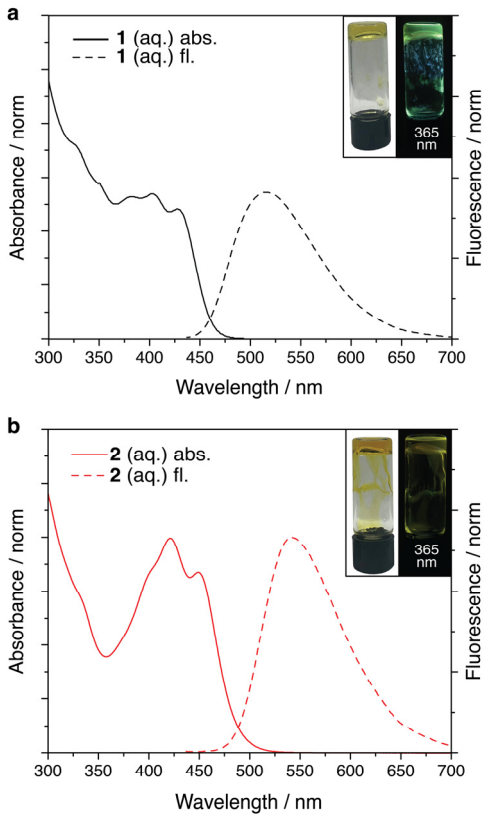

Figure 4. Photophysical properties of the self-assembled diareno-fused ullazine amphiphiles **1** and **2** in aqueous solutions. Absorption (full lines) and emission profiles (dashed lines) for self-assembled diareno-ullazines **1** and **2** gels (15 mM in 50 mM aq. NaCl solution). The insets show photographs of the gels from **1** and **2** under ambient light (left) and under 365 nm handheld lamp (right).

Next, we investigated the structures formed by ullazine amphiphiles **1** and **2** in water, where the self-assembly is driven by the stacking of the hydrophobic cores, as observed by single-crystal X-ray diffraction. Cryogenic transmission electron microscopy (cryo-TEM) of ullazines **1** and **2** in water revealed the formation of fibers several microns long (Figures 5a,b). Atomic force microscopy (AFM) also showed fiber formation with an average height of 5.5 ±0.7 nm for **1** and 3.9 ±0.3 nm for **2** (Figure 5c,d). Scanning electron microscopy (SEM) of each of the freeze-dried

gel samples (Figure S30) revealed a network of entangled fibers (and the presence of some sheets due to the freeze-drying process during sample preparation).

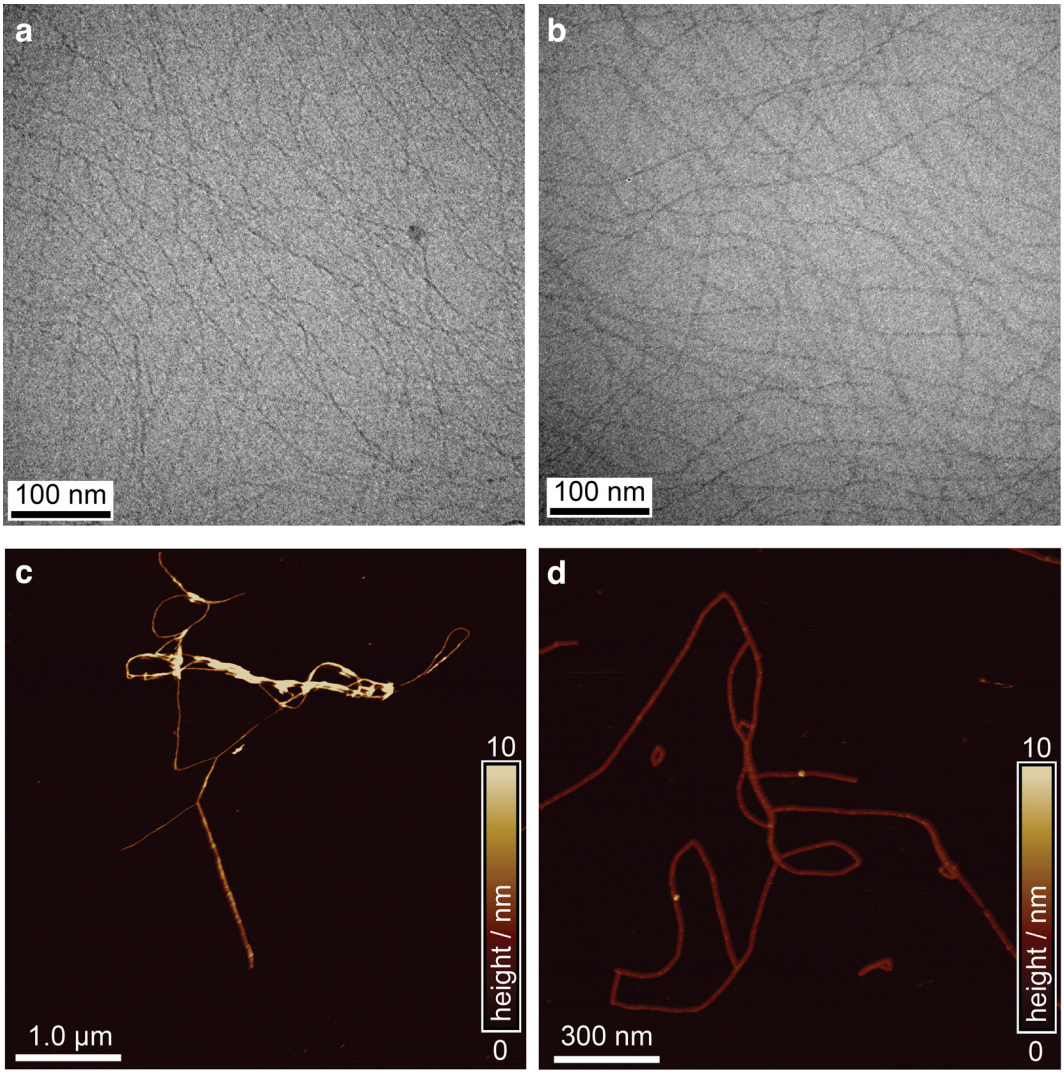

Figure 5. Micrographs of self-assembled nanostructures of **1** and **2**. Cryo-TEM of **1** (a) and **2** (b); AFM height images of **1** (c) and **2** (d).

To complement the microscopic characterization and to propose the self-assembly of monomers into supramolecular fibrous structures (Figure 6a), we carried out synchrotron solution X-ray scattering of both gels. The solution small-angle X-ray scattering (SAXS) plots of the supramolecular assembly of chromophore amphiphiles **1** and **2** in water have a slope of around −0.7 in the low q region, indicating the existence of long and/or aggregated fibers within the gel (Figure 6b). Furthermore, we observed a scattering minimum (0.17 $Å^{-1}$) that corresponds to 4 nm, in agreement with the diameter of the fiber observed by AFM. Wide-angle X-ray scattering

(WAXS) revealed in both **1** and **2** a single peak at 1.81 $Å^{-1}$ (Figure 6c), corresponding to the π–π stacking distance between chromophore cores.

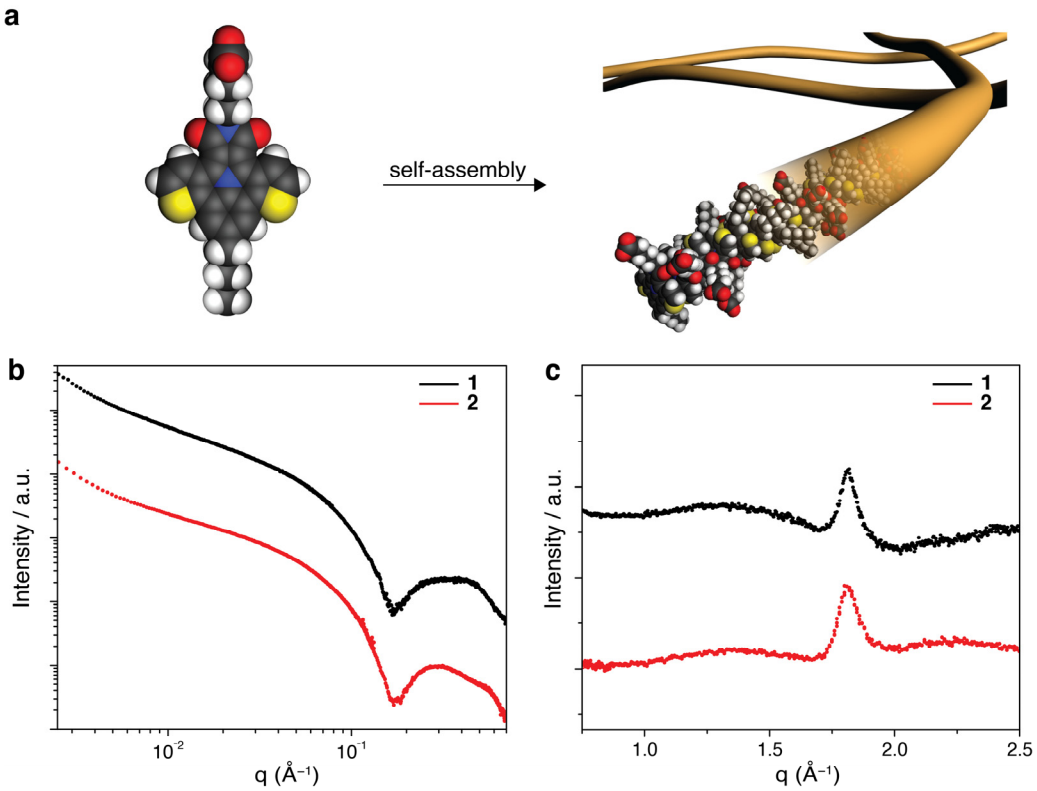

Figure 6. Self-assembled diareno-fused ullazines and solution scattering data of **1** and **2** in water. a) Molecular graphics representation of the assembly of chromophore amphiphile **2** into supramolecular fibrous structures; b) solution small and medium angle X-ray scattering curves and c) solution wide-angle X-ray scattering of self-assembled diareno-fused ullazines **1** and **2** (15 mM, 50 mM aq. NaCl).

Photocatalytic Activity. The photocatalytic reduction of CO_2 requires light absorption by a sensitizer (here: the hydrogels) and the subsequent transfer of two or eight electrons to a molecular catalyst for its reduction to carbon monoxide or methane, respectively. In designing an artificial photosynthetic systems for the photoreduction of CO_2, we coupled the photosensitizing hydrogels with CO_2-reducing non-precious metal-organic catalysts that fulfill the criteria of (*i*) suitable CO_2-reduction potentials aligned with the excited state reduction potential of ullazines, and (*ii*) partial water solubility to co-assemble with the supramolecular hydrogels. While screening with the cationic Fe-porphyrin Fe-*p*-TMA,[67] and the anionic Co-porphyrin Co-TPPS[50] gave low turnover numbers (TON, see Table S8), we found high activity of dinuclear Co-based complex catalysts, which previously showed high turnover numbers and have been recently used in aqueous solutions

(Supporting Information, Section S12).[44,45,49] Specifically, we have focused on photosensitizing two CO_2 reduction catalysts, CoCo-**1** and CoCo-**2** (Figure 7c), with our self-assembled materials.[44,49] The onset potential for the reduction of CO_2 for these catalysts are much more positive ($E_{red,CO2}$(CoCo-**1**) = −0.88 V and $E_{red,CO2}$(CoCo-**2**) = −1.0 V vs. Ag/AgCl)[44,49] than the reduction potentials of diareno-fused ullazines (E_{red}(**1**) = −1.83 V and E_{red}(**2**) = −1.79 V vs. Ag/AgCl, see Figure 2b). CoCo-**1** was chosen as a benchmark system that was reproduced by others[68] and CoCo-**2** was used because of its catalytic activity in fully aqueous solutions.[49] The most catalytically active Co-based cryptands require solvents that are mixtures of water and organic solvents such as acetonitrile (CH_3CN). Since the nanofiber assemblies in our hydrogels can be partially soluble in CH_3CN, we cross-linked the negatively charged assemblies with a positively-charged polymer,[1] poly(diallyldimethylammonium chloride), before adding the mixed solvent system. We then added to the supramolecular materials either CH_3CN/H_2O mixture or H_2O (with 0.1 M $NaHCO_3$), triethanolamine (TEAO, 0.3 M) as sacrificial donor and CoCo-**1** or CoCo-**2** (25 nM), followed by purging with CO_2 gas (for the detailed procedure, see the Supporting Information Section S12). Photoirradiation at the lowest energy absorption band of ullazine **2** hydrogel with blue light (Figure 4b, 450 nm, 200 mW cm^{-2}) for 48 h resulted in the successful reduction of CO_2 to CO and CH_4 (Figure 7a). The benchmark system, which utilized a ruthenium-based photosensitizer [RuPS or $Ru(phen)_3(PF_6)_2$] (TON_{CO} = 3747±85, TON_{CH4} = 911±170, and TON_{H2} = 31±1), and the supramolecular-based photocatalytic systems revealed comparable activity. Using self-assembled nanofibers of **1** and **2** we obtained TON_{CO} = 1136±81, TON_{CH4} = 490±132, and TON_{H2} = 12±2, and TON_{CO} = 1525±84, TON_{CH4} = 865±137 and TON_{H2} = 11±1, respectively. It is important to note that we successfully reproduced the literature value for the RuPS and CoCo-**1** system only using highly vigorous stirring (TON_{CO} = 15500 but without any CH_4 previously reported),[44] while our supramolecular systems are just irradiated without any stirring or shaking, which can disrupt the hydrogels, especially under longer irradiation times. For this reason, we compared the catalytic data with the homogenous system using the same conditions. We then investigated the fully aqueous systems employing the water-soluble catalyst CoCo-**2**.[49] Using Ru-based photosensitizers [either $Ru(phen)_3(PF_6)_2$ or $Ru(phen)_3Cl_2$] we did not observe any photoreduction products of CO_2. However, the self-assembled ullazine-based systems **1** and **2** produced both CO and CH_4 even in fully aqueous media.

While it is known that the RuPS systems become inactive after relatively short irradiation times due to photobleaching effects (around 12 to 20 h),[44,45] we investigated the effect of prolonged irradiation on the self-assembled ullazine-based system. For the time-dependent photocatalysis, we focused on the ullazine **2** system, since it was found more photocatalytically active for both CoCo catalysts. Indeed, our self-assembled photocatalytic system is able to operate for much longer periods, continuously converting CO_2 to CO and CH_4 for at least 6 days (Figure 7b and Figure S34). Importantly, after 6 days of irradiation, the supramolecular photocatalytic systems yielded greater amounts of CO_2 photoreduction products than the RuPS photosensitizer, with the ullazine-based amphiphile **2** reaching a TON_{CO} = 4645±306, TON_{CH4} = 1518±205, and TON_{H2} = 26±3. The fully aqueous system using ullazine **2** retained its activity over 6 days generating TON_{CO} = 3178±917, TON_{CH4} = 723±161 and TON_{H2} = 38±8. Again, we observed negligible production of H_2, which is a known unselective side-reaction when performing experiments in aqueous media.[30]

Finally, we investigated the photocatalytic mechanism of our supramolecular systems, which was only possible with the use of non-crosslinked hydrogels in conjunction with the water-soluble catalyst CoCo-**2** (Figure 7c) obtaining homogenous hydrogels and a decreased light scattering level. Emission experiments revealed quenching between photoexcited hydrogel **2** (or **2***) and the sacrificial donor (TEAO), supporting an oxidative electron transfer from the amine donor to the excited state of ullazine (forming $\mathbf{2}^{\bullet-}$) and suggesting a reductive quenching cycle (Figure 7d, Figure S35). Control emission quenching experiments of self-assembled **2** with CoCo-**2** did not show any emission quenching (Figure S35), suggesting that the system does not operate under an oxidative quenching pathway. The photosensitizer can therefore act as a reductant and can donate electrons to the CoCo catalysts for carbon dioxide reduction.

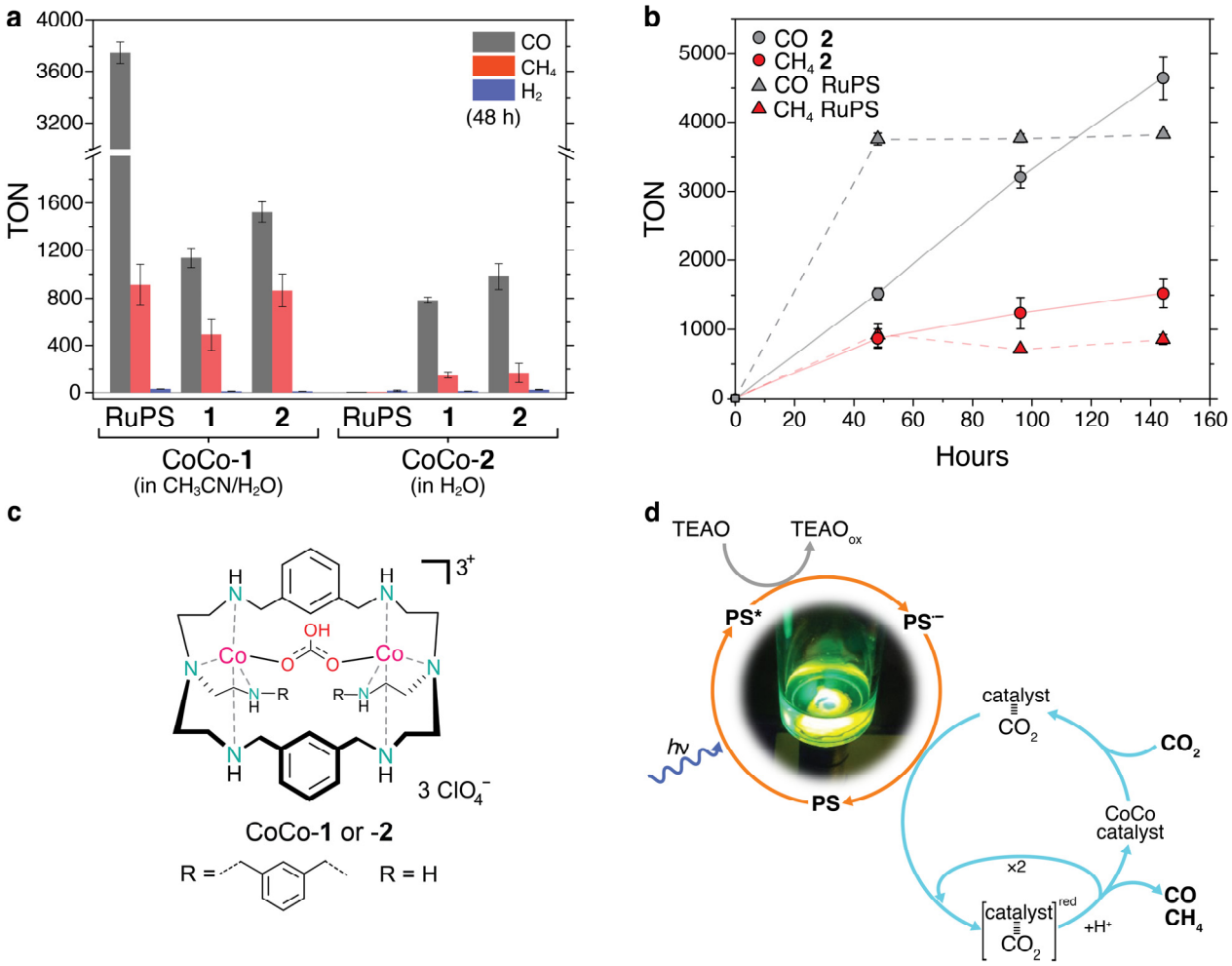

Figure 7. Photocatalytic performance of diareno-fused ullazines **1** and **2** supramolecular polymers with molecular catalysts for CO_2 reduction. a) Catalytic turnovers in CO (grey), CH_4 (red) and H_2 (blue) for using as photosensitizers $Ru(phen)_3(PF_6)_2$ (RuPS) or either **1** or **2**, with dinuclear cobalt complexes **1** [TEAO sacrificial donor (0.3 M) and catalyst (25 nM) in CH_3CN/H_2O (4:1 *v*/*v*)] and **2** [$NaHCO_3$ (0.1 M), TEAO sacrificial donor (0.3 M) and catalyst (25 nM) in H_2O] irradiated at 450 nm (200 mW cm^{-2}) for 48 hours without no shaking or stirring; b) generation of CO (grey symbols), CH_4 (red symbols) with time (48, 96 and 144 hours) for diareno-fused ullazine **2** and CoCo-**1** (under the same conditions used in panel a, CH_3CN/H_2O, 4:1 *v*/*v*); c) chemical structures of the two dicobalt cryptands CO_2 reduction catalysts ; d) proposed mechanism for the reduction of CO_2 to CO and CH_4 by self-assembled diareno-fused ullazines photosensitizers (PS) and dinuclear cobalt complexes (the photograph is of a vial containing self-assembled **1** cross-linked with PDDA in aqueous solution and irradiated with 450 nm LED).

Conclusions

We have developed two novel supramolecular polymers based on diareno-fused ullazines chromophore amphiphiles **1** and **2** that can sensitize dicobalt catalysts for the CO_2 reduction to CO

and CH_4 under irradiation with visible light. The rational design of the chromophore core based on its excited state reduction potential and visible light absorption properties was incorporated into an amphiphilic self-assembled material acting as an efficient photosensitizer. The π-stacked supramolecular fibers sensitize Co-based molecular catalysts with comparable efficiency to a precious metal complex in aqueous organic media (CH_3CN/H_2O 4:1 *v*/*v*). The catalytic activity of these supramolecular gels even outperforms turnover numbers of a comparable system sensitized with $Ru(phen)_3(PF_6)_2$ with respect to CO and CH_4 production in fully aqueous media. Prolonged activities over 6 days further complement the performance of these organic sensitizers. We envision that future catalytic transformations of even more complex organic substrates could be sensitized with self-assembled soft materials under environmentally feasible conditions. This combined strategy of self-assembling rationally designed chromophores to create functional soft materials could become a general approach towards tailored photocatalytic systems and solar energy materials.

ASSOCIATED CONTENT

SUPPORTING INFORMATION

The Supporting Information is available free of charge on the ACS Publications website.
Detailed information on experimental methods, materials used, synthetic characterization, calculations, and data (PDF)
X-ray crystallographic data for **1** (CCDC-1878616) (CIF)
X-ray crystallographic data for **2** (CCDC-1878614) (CIF)
X-ray crystallographic data for **S2** (CCDC-1878609) (CIF)
X-ray crystallographic data for **CoCo-1** (CCDC-1878608) (CIF)

AUTHOR INFORMATION

Corresponding author

Correspondence to Samuel I. Stupp. E-mail: s-stupp@northwestern.edu

Author Contributions

[†]O.D. and L.Đ. contributed equally.

ACKNOWLEDGMENTS

This work was supported by the Center for Bio-Inspired Energy Science (CBES), an Energy Frontier Research Center (EFRC) funded by the US Department of Energy, Office of Science, Basic Energy Sciences under award number DE-SC0000989. O.D. acknowledges funding by the Swiss National Science Foundation (SNF, project P2EZP2_168881) via an Early Postdoc.Mobility fellowship and the National Academy of Sciences Leopoldina (Germany) for a postdoctoral fellowship (LPDS 2016-4). Use of the Advanced Photon Source (APS) was supported by the Basic Energy Sciences program of the US Department of Energy Office of Science under contract no. DE-AC02-06CH11357. Angle-dependent X-ray experiments were performed at the DuPont-Northwestern-Dow Collaborative Access Team (DND-CAT) located at Sector 5 of the APS. DND-CAT is supported by Northwestern University, E.I. DuPont de Nemours & Co., and the Dow Chemical Company. We thank the Biological Imaging Facility at Northwestern for the use of TEM equipment and the Electron Probe Instrumentation Center facilities of the Northwestern University Atomic and Nanoscale Characterization Experimental Center for the use of TEM and SEM equipment. Single-crystal X-ray diffraction, NMR and mass spectroscopy equipment at the Integrated Molecular Structure Education and Research Center was supported by the National Science Foundation under CHE-9871268. We thank Charlotte Stern for crystallographic advice. The authors would also like to thank Mark Seniw for his help in preparing the schematics used in the manuscript.

REFERENCES

(1) Weingarten, A. S.; Kazantsev, R. V.; Palmer, L. C.; McClendon, M.; Koltonow, A. R.; Samuel, A. P. S.; Kiebala, D. J.; Wasielewski, M. R.; Stupp, S. I. Self-Assembling Hydrogel Scaffolds for Photocatalytic Hydrogen Production. *Nat. Chem.* **2014**, *6* (11), 964–970. https://doi.org/10.1038/nchem.2075.

(2) Dumele, O.; Chen, J.; Passarelli, J. V.; Stupp, S. I. Supramolecular Energy Materials. *Adv. Mater.* **2020**, *32* (17), 1907247. https://doi.org/10.1002/adma.201907247.

(3) Wasielewski, M. R. Self-Assembly Strategies for Integrating Light Harvesting and Charge Separation in Artificial Photosynthetic Systems. *Acc. Chem. Res.* **2009**, *42* (12), 1910–1921. https://doi.org/10.1021/ar9001735.

(4) Kunz, V.; Stepanenko, V.; Würthner, F. Embedding of a Ruthenium(II) Water Oxidation Catalyst into Nanofibers via Self-Assembly. *Chem. Commun.* **2015**, *51* (2), 290–293. https://doi.org/10.1039/c4cc08314h.

(5) Ishiwari, F.; Shoji, Y.; Fukushima, T. Supramolecular Scaffolds Enabling the Controlled Assembly of Functional Molecular Units. *Chem. Sci.* **2018**, *9* (8), 2028–2041. https://doi.org/10.1039/c7sc04340f.

(6) Xu, C.; Ravi Anusuyadevi, P.; Aymonier, C.; Luque, R.; Marre, S. Nanostructured Materials for Photocatalysis. *Chem. Soc. Rev.* **2019**, *48* (14), 3868–3902. https://doi.org/10.1039/c9cs00102f.

(7) Zhao, F.; Bae, J.; Zhou, X.; Guo, Y.; Yu, G. Nanostructured Functional Hydrogels as an Emerging Platform for Advanced Energy Technologies. *Adv. Mater.* **2018**, *30* (48), 1801796. https://doi.org/10.1002/adma.201801796.

(8) Keijer, T.; Bouwens, T.; Hessels, J.; Reek, J. N. H. Supramolecular Strategies in Artificial Photosynthesis. *Chem. Sci.* **2021**, *12* (1), 50–70. https://doi.org/10.1039/D0SC03715J.

(9) Bhattacharyya, A.; De Sarkar, S.; Das, A. Supramolecular Engineering and Self-Assembly Strategies in Photoredox Catalysis. *ACS Catal.* **2021**, *11* (2), 710–733. https://doi.org/10.1021/acscatal.0c04952.

(10) Abramov, A.; Bonardd, S.; Pérez-Ruiz, R.; Díaz Díaz, D. Recyclable, Immobilized Transition-Metal Photocatalysts. *Adv. Synth. Catal.* **2022**, *364* (1), 2–17. https://doi.org/10.1002/adsc.202101048.

(11) Biswas, S.; Kumar, M.; Levine, A. M.; Jimenez, I.; Ulijn, R. V.; Braunschweig, A. B. Visible-Light Photooxidation in Water by $^1O_2$-Generating Supramolecular Hydrogels. *Chem. Sci.* **2020**, *11* (16), 4239–4245. https://doi.org/10.1039/c9sc06481h.

(12) Tian, J.; Zhang, Y.; Du, L.; He, Y.; Jin, X.-H.; Pearce, S.; Eloi, J.-C.; Harniman, R. L.; Alibhai, D.; Ye, R.; Phillips, D. L.; Manners, I. Tailored Self-Assembled Photocatalytic Nanofibres for Visible-Light-Driven Hydrogen Production. *Nat. Chem.* **2020**, *12* (12), 1150–1156. https://doi.org/10.1038/s41557-020-00580-3.

(13) Chen, Y.; Yan, C.; Dong, J.; Zhou, W.; Rosei, F.; Feng, Y.; Wang, L. Structure/Property Control in Photocatalytic Organic Semiconductor Nanocrystals. *Adv. Funct. Mater.* **2021**, *31* (36), 2104099. https://doi.org/10.1002/adfm.202104099.

(14) Hestand, N. J.; Kazantsev, R. V.; Weingarten, A. S.; Palmer, L. C.; Stupp, S. I.; Spano, F. C. Extended-Charge-Transfer Excitons in Crystalline Supramolecular Photocatalytic

Scaffolds. *J. Am. Chem. Soc.* **2016**, *138* (36), 11762–11774. https://doi.org/10.1021/jacs.6b05673.

(15) Kazantsev, R. V.; Dannenhoffer, A. J.; Aytun, T.; Harutyunyan, B.; Fairfield, D. J.; Bedzyk, M. J.; Stupp, S. I. Molecular Control of Internal Crystallization and Photocatalytic Function in Supramolecular Nanostructures. *Chem* **2018**, *4* (7), 1596–1608. https://doi.org/10.1016/j.chempr.2018.04.002.

(16) Sai, H.; Lau, G. C.; Dannenhoffer, A. J.; Chin, S. M.; Đorđević, L.; Stupp, S. I. Imaging Supramolecular Morphogenesis with Confocal Laser Scanning Microscopy at Elevated Temperatures. *Nano Lett.* **2020**, *20* (6), 4234–4241. https://doi.org/10.1021/acs.nanolett.0c00662.

(17) Dannenhoffer, A. J.; Sai, H.; Harutyunyan, B.; Narayanan, A.; Powers-Riggs, N. E.; Edelbrock, A. N.; Passarelli, J. V.; Weigand, S. J.; Wasielewski, M. R.; Bedzyk, M. J.; Palmer, L. C.; Stupp, S. I. Growth of Extra-Large Chromophore Supramolecular Polymers for Enhanced Hydrogen Production. *Nano Lett.* **2021**, *21* (9), 3745–3752. https://doi.org/10.1021/acs.nanolett.0c05024.

(18) Yang, G.; Lin, C.; Feng, X.; Wang, T.; Jiang, J. Multi-Component Supramolecular Gels Induce Protonation of a Porphyrin Exciplex to Achieve Improved Collective Optical Properties for Effective Photocatalytic Hydrogen Generation. *Chem. Commun.* **2020**, *56* (4), 527–530. https://doi.org/10.1039/c9cc08060k.

(19) Liu, Y.; Wang, L.; Feng, H.; Ren, X.; Ji, J.; Bai, F.; Fan, H. Microemulsion-Assisted Self-Assembly and Synthesis of Size-Controlled Porphyrin Nanocrystals with Enhanced Photocatalytic Hydrogen Evolution. *Nano Lett.* **2019**, *19* (4), 2614–2619. https://doi.org/10.1021/acs.nanolett.9b00423.

(20) Gueret, R.; Poulard, L.; Oshinowo, M.; Chauvin, J.; Dahmane, M.; Dupeyre, G.; Lainé, P. P.; Fortage, J.; Collomb, M. N. Challenging the [Ru(Bpy)3]2+ Photosensitizer with a Triazatriangulenium Robust Organic Dye for Visible-Light-Driven Hydrogen Production in Water. *ACS Catal.* **2018**, *8* (5), 3792–3802. https://doi.org/10.1021/acscatal.7b04000.

(21) Yang, X.; Hu, Z.; Yin, Q.; Shu, C.; Jiang, X. F.; Zhang, J.; Wang, X.; Jiang, J. X.; Huang, F.; Cao, Y. Water-Soluble Conjugated Molecule for Solar-Driven Hydrogen Evolution from Salt Water. *Adv. Funct. Mater.* **2019**, *29* (13), 1808156. https://doi.org/10.1002/adfm.201808156.

(22) Liu, D.; Wang, J.; Bai, X.; Zong, R.; Zhu, Y. Self-Assembled PDINH Supramolecular

System for Photocatalysis under Visible Light. *Adv. Mater.* **2016**, *28* (33), 7284–7290. https://doi.org/10.1002/adma.201601168.

(23) Nolan, M. C.; Walsh, J. J.; Mears, L. L. E.; Draper, E. R.; Wallace, M.; Barrow, M.; Dietrich, B.; King, S. M.; Cowan, A. J.; Adams, D. J. PH Dependent Photocatalytic Hydrogen Evolution by Self-Assembled Perylene Bisimides. *J. Mater. Chem. A* **2017**, *5* (16), 7555–7563. https://doi.org/10.1039/c7ta01845b.

(24) McDowall, D.; Greeves, B. J.; Clowes, R.; McAulay, K.; Fuentes-Caparrós, A. M.; Thomson, L.; Khunti, N.; Cowieson, N.; Nolan, M. C.; Wallace, M.; Cooper, A. I.; Draper, E. R.; Cowan, A. J.; Adams, D. J. Controlling Photocatalytic Activity by Self-Assembly – Tuning Perylene Bisimide Photocatalysts for the Hydrogen Evolution Reaction. *Adv. Energy Mater.* **2020**, *10* (46), 2002469. https://doi.org/10.1002/aenm.202002469.

(25) Jiao, X.; Zheng, K.; Hu, Z.; Sun, Y.; Xie, Y. Broad-Spectral-Response Photocatalysts for CO_2 Reduction. *ACS Cent. Sci.* **2020**, *6* (5), 653–660. https://doi.org/10.1021/acscentsci.0c00325.

(26) Fernández, J. R.; Garcia, S.; Sanz-Pérez, E. S. CO_2 Capture and Utilization Editorial. *Ind. Eng. Chem. Res.* **2020**, *59* (15), 6767–6772. https://doi.org/10.1021/acs.iecr.0c01643.

(27) Appel, A. M.; Bercaw, J. E.; Bocarsly, A. B.; Dobbek, H.; Dubois, D. L.; Dupuis, M.; Ferry, J. G.; Fujita, E.; Hille, R.; Kenis, P. J. A.; Kerfeld, C. A.; Morris, R. H.; Peden, C. H. F.; Portis, A. R.; Ragsdale, S. W.; Rauchfuss, T. B.; Reek, J. N. H.; Seefeldt, L. C.; Thauer, R. K.; Waldrop, G. L. Frontiers, Opportunities, and Challenges in Biochemical and Chemical Catalysis of CO_2 Fixation. *Chem. Rev.* **2013**, *113* (8), 6621–6658. https://doi.org/10.1021/cr300463y.

(28) Aresta, M.; Dibenedetto, A.; Angelini, A. Catalysis for the Valorization of Exhaust Carbon: From CO2 to Chemicals, Materials, and Fuels. Technological Use of CO_2. *Chem. Rev.* **2014**, *114* (3), 1709–1742. https://doi.org/10.1021/cr4002758.

(29) He, J.; Janáky, C. Recent Advances in Solar-Driven Carbon Dioxide Conversion: Expectations versus Reality. *ACS Energy Lett.* **2020**, *5* (6), 1996–2014. https://doi.org/10.1021/acsenergylett.0c00645.

(30) Takeda, H.; Cometto, C.; Ishitani, O.; Robert, M. Electrons, Photons, Protons and Earth-Abundant Metal Complexes for Molecular Catalysis of CO_2 Reduction. *ACS Catal.* **2017**, *7* (1), 70–88. https://doi.org/10.1021/acscatal.6b02181.

(31) Ulmer, U.; Dingle, T.; Duchesne, P. N.; Morris, R. H.; Tavasoli, A.; Wood, T.; Ozin, G. A.

Fundamentals and Applications of Photocatalytic CO_2 Methanation. *Nat. Commun.* **2019**, *10* (1), 3169. https://doi.org/10.1038/s41467-019-10996-2.

(32) Dalle, K. E.; Warnan, J.; Leung, J. J.; Reuillard, B.; Karmel, I. S.; Reisner, E. Electro- and Solar-Driven Fuel Synthesis with First Row Transition Metal Complexes. *Chem. Rev.* **2019**, *119* (4), 2752–2875. https://doi.org/10.1021/acs.chemrev.8b00392.

(33) Barber, J. Photosynthetic Energy Conversion: Natural and Artificial. *Chem. Soc. Rev.* **2009**, *38* (1), 185–196. https://doi.org/10.1039/b802262n.

(34) Woolerton, T. W.; Sheard, S.; Chaudhary, Y. S.; Armstrong, F. A. Enzymes and Bio-Inspired Electrocatalysts in Solar Fuel Devices. *Energy Environ. Sci.* **2012**, *5* (6), 7470–7490. https://doi.org/10.1039/c2ee21471g.

(35) Nocera, D. G. The Artificial Leaf. *Acc. Chem. Res.* **2012**, *45* (5), 767–776. https://doi.org/10.1021/ar2003013.

(36) Zhang, B.; Sun, L. Artificial Photosynthesis: Opportunities and Challenges of Molecular Catalysts. *Chem. Soc. Rev.* **2019**, *48* (7), 2216–2264. https://doi.org/10.1039/c8cs00897c.

(37) Reisner, E. When Does Organic Photoredox Catalysis Meet Artificial Photosynthesis? *Angew. Chem. Int. Ed.* **2019**, *58* (12), 3656–3657. https://doi.org/10.1002/anie.201814692.

(38) Lehn, J.-M.; Ziessel, R. Photochemical Generation of Carbon Monoxide and Hydrogen by Reduction of Carbon Dioxide and Water under Visible Light Irradiation. *Proc. Natl. Acad. Sci.* **1982**, *79* (2), 701–704. https://doi.org/10.1073/pnas.79.2.701.

(39) Wang, F. Artificial Photosynthetic Systems for CO_2 Reduction: Progress on Higher Efficiency with Cobalt Complexes as Catalysts. *ChemSusChem* **2017**, *10* (22), 4393–4402. https://doi.org/10.1002/cssc.201701385.

(40) Rao, H.; Lim, C. H.; Bonin, J.; Miyake, G. M.; Robert, M. Visible-Light-Driven Conversion of CO_2 to CH_4 with an Organic Sensitizer and an Iron Porphyrin Catalyst. *J. Am. Chem. Soc.* **2018**, *140* (51), 17830–17834. https://doi.org/10.1021/jacs.8b09740.

(41) Wisser, F. M.; Duguet, M.; Perrinet, Q.; Ghosh, A. C.; Alves-Favaro, M.; Mohr, Y.; Lorentz, C.; Quadrelli, E. A.; Palkovits, R.; Farrusseng, D.; Mellot-Draznieks, C.; de Waele, V.; Canivet, J. Molecular Porous Photosystems Tailored for Long-Term Photocatalytic CO_2 Reduction. *Angew. Chem. Int. Ed.* **2020**, *59* (13), 5116–5122. https://doi.org/10.1002/anie.201912883.

(42) Ma, B.; Chen, G.; Fave, C.; Chen, L.; Kuriki, R.; Maeda, K.; Ishitani, O.; Lau, T. C.; Bonin, J.; Robert, M. Efficient Visible-Light-Driven CO_2 Reduction by a Cobalt Molecular

Catalyst Covalently Linked to Mesoporous Carbon Nitride. *J. Am. Chem. Soc.* **2020**, *142* (13), 6188–6195. https://doi.org/10.1021/jacs.9b13930.

(43) Shirley, H.; Su, X.; Sanjanwala, H.; Talukdar, K.; Jurss, J. W.; Delcamp, J. H. Durable Solar-Powered Systems with Ni-Catalysts for Conversion of CO_2 or CO to CH_4. *J. Am. Chem. Soc.* **2019**, *141* (16), 6617–6622. https://doi.org/10.1021/jacs.9b00937.

(44) Ouyang, T.; Huang, H. H.; Wang, J. W.; Zhong, D. C.; Lu, T. B. A Dinuclear Cobalt Cryptate as a Homogeneous Photocatalyst for Highly Selective and Efficient Visible-Light Driven CO_2 Reduction to CO in CH_3CN/H_2O Solution. *Angew. Chem. Int. Ed.* **2017**, *56* (3), 738–743. https://doi.org/10.1002/anie.201610607.

(45) Ouyang, T.; Wang, H. J.; Huang, H. H.; Wang, J. W.; Guo, S.; Liu, W. J.; Zhong, D. C.; Lu, T. B. Dinuclear Metal Synergistic Catalysis Boosts Photochemical CO_2-to-CO Conversion. *Angew. Chem. Int. Ed.* **2018**, *57* (50), 16480–16485. https://doi.org/10.1002/anie.201811010.

(46) Zhang, X.; Cibian, M.; Call, A.; Yamauchi, K.; Sakai, K. Photochemical CO_2 Reduction Driven by Water-Soluble Copper(I) Photosensitizer with the Catalysis Accelerated by Multi-Electron Chargeable Cobalt Porphyrin. *ACS Catal.* **2019**, *9* (12), 11263–11273. https://doi.org/10.1021/acscatal.9b04023.

(47) Chen, Y.; Li, P.; Zhou, J.; Buru, C. T.; Đorđević, L.; Li, P.; Zhang, X.; Cetin, M. M.; Stoddart, J. F.; Stupp, S. I.; Wasielewski, M. R.; Farha, O. K. Integration of Enzymes and Photosensitizers in a Hierarchical Mesoporous Metal–Organic Framework for Light-Driven CO 2 Reduction. *J. Am. Chem. Soc.* **2020**, *142* (4), 1768–1773. https://doi.org/10.1021/jacs.9b12828.

(48) Arcudi, F.; Đorđević, L.; Nagasing, B.; Stupp, S. I.; Weiss, E. A. Quantum Dot-Sensitized Photoreduction of CO 2 in Water with Turnover Number > 80,000. *J. Am. Chem. Soc.* **2021**, *143* (43), 18131–18138. https://doi.org/10.1021/jacs.1c06961.

(49) Bi, Q. Q.; Wang, J. W.; Lv, J. X.; Wang, J.; Zhang, W.; Lu, T. B. Selective Photocatalytic CO_2 Reduction in Water by Electrostatic Assembly of CdS Nanocrystals with a Dinuclear Cobalt Catalyst. *ACS Catal.* **2018**, *8* (12), 11815–11821. https://doi.org/10.1021/acscatal.8b03457.

(50) Call, A.; Cibian, M.; Yamamoto, K.; Nakazono, T.; Yamauchi, K.; Sakai, K. Highly Efficient and Selective Photocatalytic CO_2 Reduction to CO in Water by a Cobalt Porphyrin Molecular Catalyst. *ACS Catal.* **2019**, *9* (6), 4867–4874.

https://doi.org/10.1021/acscatal.8b04975.

(51) Stępień, M.; Gońka, E.; Żyła, M.; Sprutta, N. Heterocyclic Nanographenes and Other Polycyclic Heteroaromatic Compounds: Synthetic Routes, Properties, and Applications. *Chem. Rev.* **2017**, *117* (4), 3479–3716. https://doi.org/10.1021/acs.chemrev.6b00076.

(52) Balli, H.; Zeller, M. Neue Heteroarene: Synthese Und Spektrale Daten von Indolizino[6,5,4,3-aij]Chinolin («Ullazin») Und Einigen Derivaten. *Helv. Chim. Acta* **1983**, *66* (7), 2135–2139. https://doi.org/10.1002/hlca.19830660724.

(53) Delcamp, J. H.; Yella, A.; Holcombe, T. W.; Nazeeruddin, M. K.; Grätzel, M. The Molecular Engineering of Organic Sensitizers for Solar-Cell Applications. *Angew. Chem. Int. Ed.* **2013**, *52* (1), 376–380. https://doi.org/10.1002/anie.201205007.

(54) Miao, D.; Aumaitre, C.; Morin, J. F. Photochemical Synthesis of π-Extended Ullazine Derivatives as New Electron Donors for Efficient Conjugated D-A Polymers. *J. Mater. Chem. C* **2019**, *7* (10), 3015–3024. https://doi.org/10.1039/c8tc05288c.

(55) Cebrián, C. Ullazine-Based Materials: Towards Novel Opportunities in Organic Electronics. *J. Mater. Chem. C* **2018**, *6* (44), 11943–11950. https://doi.org/10.1039/c8tc03573c.

(56) Berger, R.; Wagner, M.; Feng, X.; Müllen, K. Polycyclic Aromatic Azomethine Ylides: A Unique Entry to Extended Polycyclic Heteroaromatics. *Chem. Sci.* **2015**, *6* (1), 436–441. https://doi.org/10.1039/c4sc02793k.

(57) Ito, S.; Tokimaru, Y.; Nozaki, K. Isoquinolino[4,3,2-de]Phenanthridine: Synthesis and Its Use in 1,3-Dipolar Cycloadditions to Form Nitrogen-Containing Polyaromatic Hydrocarbons. *Chem. Commun.* **2015**, *51* (1), 221–224. https://doi.org/10.1039/c4cc06643j.

(58) Tokimaru, Y.; Ito, S.; Nozaki, K. Synthesis of Pyrrole-Fused Corannulenes: 1,3-Dipolar Cycloaddition of Azomethine Ylides to Corannulene. *Angew. Chem. Int. Ed.* **2017**, *56* (49), 15560–15564. https://doi.org/10.1002/anie.201707087.

(59) Richter, M.; Schellhammer, K. S.; MacHata, P.; Cuniberti, G.; Popov, A.; Ortmann, F.; Berger, R.; Müllen, K.; Feng, X. Polycyclic Heteroaromatic Hydrocarbons Containing a Benzoisoindole Core. *Org. Chem. Front.* **2017**, *4* (5), 847–852. https://doi.org/10.1039/c7qo00180k.

(60) Richter, M.; Hahn, S.; Dmitrieva, E.; Rominger, F.; Popov, A.; Bunz, U. H. F.; Feng, X.; Berger, R. Helical Ullazine-Quinoxaline-Based Polycyclic Aromatic Hydrocarbons. *Chem.*

Eur. J. **2019**, *25* (5), 1345–1352. https://doi.org/10.1002/chem.201804751.

(61) Miao, D.; Di Michele, V.; Gagnon, F.; Aumaître, C.; Lucotti, A.; Del Zoppo, M.; Lirette, F.; Tommasini, M.; Morin, J. F. Pyrrole-Embedded Linear and Helical Graphene Nanoribbons. *J. Am. Chem. Soc.* **2021**, *143* (30), 11302–11308. https://doi.org/10.1021/jacs.1c05616.

(62) Richter, M.; Borkowski, M.; Fu, Y.; Dmitrieva, E.; Popov, A.; Ma, J.; Marszalek, T.; Pisula, W.; Feng, X. Synthesis and Self-Assembly Behavior of Double Ullazine-Based Polycyclic Aromatic Hydrocarbons. *Org. Mater.* **2021**, *03* (02), 198–203. https://doi.org/10.1055/a-1472-6852.

(63) Berger, R.; Giannakopoulos, A.; Ravat, P.; Wagner, M.; Beljonne, D.; Feng, X.; Müllen, K. Synthesis of Nitrogen-Doped Zigzag-Edge Peripheries: Dibenzo-9a-Azaphenalene as Repeating Unit. *Angew. Chem. Int. Ed.* **2014**, *53* (39), 10520–10524. https://doi.org/10.1002/anie.201403302.

(64) Knapp, D. M.; Gillis, E. P.; Burke, M. D. A General Solution for Unstable Boronic Acids: Slow-Release Cross-Coupling from Air-Stable MIDA Boronates. *J. Am. Chem. Soc.* **2009**, *131* (20), 6961–6963. https://doi.org/10.1021/ja901416p.

(65) Gershoni-Poranne, R.; Stanger, A. Magnetic Criteria of Aromaticity. *Chem. Soc. Rev.* **2015**, *44* (18), 6597–6615. https://doi.org/10.1039/c5cs00114e.

(66) Geuenich, D.; Hess, K.; Köhler, F.; Herges, R. Anisotropy of the Induced Current Density (ACID), a General Method to Quantify and Visualize Electronic Delocalization. *Chem. Rev.* **2005**, *105* (10), 3758–3772. https://doi.org/10.1021/cr0300901.

(67) Costentin, C.; Robert, M.; Savéant, J.-M.; Tatin, A. Efficient and Selective Molecular Catalyst for the CO_2-to-CO Electrochemical Conversion in Water. *Proc. Natl. Acad. Sci.* **2015**, *112* (22), 6882–6886. https://doi.org/10.1073/pnas.1507063112.

(68) Realista, S.; Almeida, J. C.; Milheiro, S. A.; Bandeira, N. A. G.; Alves, L. G.; Madeira, F.; Calhorda, M. J.; Martinho, P. N. CoII Cryptates Convert CO_2 into CO and CH_4 under Visible Light. *Chem. Eur. J.* **2019**, *25* (50), 11670–11679. https://doi.org/10.1002/chem.201901806.

TABLE OF CONTENT FIGURE